A lab-scale experiment to measure terminal velocity of volcanic ash

B. Andò M. Coltelli M. Prestifilippo and S. Scollo

Abstract

In this paper, a novel methodology to measure trajectory and terminal velocity of volcanic ash in laboratory is presented. The methodology consists of: i) planning a lab-scale experiment in order to reproduce the sedimentation processes of fine volcanic ash based on the principle of dynamic similarity; ii) realizing the experimental set-up using a glass tank filled with glycerine, a web-cam based vision system and a dedicated image post processing tool able to estimate the position and the terminal velocity of any particle falling in the tank; iii) performing a calibration procedure to accurately estimate the uncertainty on particle velocity; iv) comparing the experimental results with estimations obtained by some particle fallout models available in literature. Our results shows that there is a good agreement between experimental terminal velocities and those obtained applying a model which includes information on particle shape. The proposed methodology allows us to investigate how the particle shape affects the sedimentation processes. Since the latter is strategic to improve the accuracy on modeling ash fallout, this work will contribute to reduce risks to aviations during explosive eruptions.

Index Terms

Volcanic ash, lab-scale experiments, trajectory reconstruction, terminal settling velocity

Bruno Andò is with the Dipartimento di Ingegneria Elettrica Elettronica e dei Sistemi, Università degli studi di Catania, Catania (CT), 95125, Italy, Phone: (0039) 95-7382601, email: bando@diees.unict.it

Mauro Coltelli is with the Istituto Nazionale di Geofisica e Vulcanologia, sezione di Catania, Catania (CT), 95125, Italy, Phone: (0039) 95-7165800, email: coltelli@ct.ingv.it

Michele Prestifilippo is with the Istituto Nazionale di Geofisica e Vulcanologia, sezione di Catania, Catania (CT), 95125, Italy, Phone: (0039) 95-7165800, email: prestifilippo@ct.ingv.it

Simona Scollo is with the Istituto Nazionale di Geofisica e Vulcanologia, sezione di Catania, Catania (CT), 95125, Italy, Phone: (0039) 95-7165800, email: scollo@ct.ingv.it

I. Introduction

Terminal settling velocity is greatly influenced by particle size, shape, orientation and density, and in addition, by air density and viscosity. It is reached when the Drag force, the aerodynamic force that opposes its motion through the air, is equal to the gravity force and is given by [1]:

$$V_T = \sqrt{\frac{4}{3}\frac{d\left(\sigma-\rho\right)g}{C_D\rho}} \tag{1}$$

where V_T is the terminal settling velocity of the particle $(\mathrm{m/s})$, d is the particle diameter (m) that specifies the cross-sectional area of the particle, σ and ρ are the particle and air densities $(\mathrm{kg/m^3})$, g is the gravity acceleration $(\mathrm{m/s^2})$ and C_D is the Drag coefficient, a dimensionless parameter which depends on particle characteristics (e.g. size, shape) and Reynolds number R_e:

$$R_e = \frac{\rho d V_T}{\mu} \tag{2}$$

where μ is the dynamic viscosity $(\mathrm{kg/sm})$.

Although the knowledge on settling behavior of spherical particles in compressible and incompressible viscous media was established in the last century, the free settling behavior of non-spherical particles is still poorly known. Theoretical treatments are limited to well-defined shapes and/or to well-defined flow regimes [2], whereas the terminal settling velocity of irregular particles such as volcanic ash needs to be evaluated empirically [3]. The pioneer work carried out to investigate the terminal settling velocity of volcanic particles is presented in [4]. Particles larger than $5\ \mathrm{mm}$ were measured and they fell more similarly to cylinders than to spheres. The fall velocity of a great number of volcanic particles with mean diameters between $20\ \mu\mathrm{m}$ and $500\ \mu\mathrm{m}$ were then measured in [5]. Volcanic particles fell into a vertical tube and were illuminated by a commercial stroboscope (flashing at $100 \pm 0.5\ \mathrm{Hz}$). When particles came out of the tube, they were photographed with a camera; afterward terminal settling velocities were evaluated. Two tubes of

$120\ \mathrm{mm}$ and $317\ \mathrm{mm}$ (for the larger particles) in length were used to assure that particles reached 85% of their terminal settling velocity. Data obtained from this experiment were used to empirically find the C_D value for volcanic particles based on a shape parameter F and R_e:

$$C_D = \frac{24}{R_e} F^{-0.32} + 2\sqrt{1.07 - F} \tag{3}$$

where $F = (b + c)/2a$ is calculated using a, b, c, the three principal axial lengths ($a > b > c$), and $d = (a + b + c)/3$. Wilson and Huang evaluated the terminal settling velocities (VWH) using (1). It is highlighted that VWH are lower than those calculated assuming particles as spheres.

Another experiment is presented in [6]. The authors measured size, shape and terminal settling velocity of 2500 particles having a diameter between $10\ \mu\mathrm{m}$ and $150\ \mu\mathrm{m}$ and coming from three distal fallout deposits of Fuego Volcano, Mount Spurr Volcano and Ash Hollow Member. The particle size was measured using laser diffraction analysis, the characterization of the particle shape by analyzing images taken by SEM as well as the measurements of the particle surface area by the BET method. Finally, the Roller particles size analyzer [7], able to sort particles into terminal settling velocity groups between $0.6\ \mathrm{cm/s}$ and $59.0\ \mathrm{cm/s}$, was used to evaluate their terminal settling velocities. These authors [6] showed that the most useful descriptors of particle shape were aspect ratio, Feret diameter and perimeter measurements and that, similar to results reported in [5], the diameters of ash particles were $10 - 120\%$ larger than ideal spheres falling at the same terminal settling velocity.

Other authors [8] measured V_T of particles produced during explosive eruptions of Vesuvio and Campi Flegrei (Italy). Grain-size measurements were performed by combining sieving and particle-counting techniques, the particle density was performed by standard Gay-Lussac picnometres, and finally shape parameters were measured by using image analysis techniques on high-resolution digital photographs of particles mounted on a goniometric universal stage under a stereomicroscope [8]. Particles fell into a box of distilled water and ethylic alcohol at $293\mathrm{K}$ and their velocities were analyzed using films obtained by a 3CCD progressive scan camera. Hence, they found a new formula to predict V_T of pumice particles and estimated an average error of 12% with respect to the experimental results:

$$V_T = \frac{1.2065\mu\left(d^3 g\left(\sigma-\rho\right)\sigma\Psi^{1.6}/\mu^2\right)^{0.5026}}{d\rho} \tag{4}$$

where Ψ is a shape factor, defined as the ratio of sphericity to circularity. The sphericity is ratio between the surface area of the equivalent sphere and the surface area of the actual particle, whereas the circularity is the ratio between the particle perimeter and the perimeter of the circle equivalent to the maximum projected area. Recently, the shape of 2065 volcanic ash erupted during 2002-03 Etna eruption was measured using SEM image analysis [9]. Kunii and Levenspiel calculated the terminal settling velocity (VKL) using the model treated in [10]:

$$V_{KL} = \begin{cases} g\sigma d^2/18\mu & R_e \leq 0.4 \\ d\left(4g^2\sigma^2/225\rho\mu\right)^{\frac{1}{3}} & 0.4 < R_e \leq 500 \\ \left(3.1g\sigma d/\rho\right)^{\frac{1}{2}} & R_e > 500 \end{cases} \tag{5}$$

and compared these values with VWH measuring the aspect ratio of real volcanic particles. They found that VKL were on average 1.28 greater than VWH and the differences ranged between 20% and 90%, highlighting again how the particle shape influences the terminal settling velocity.

In this work, a new strategy able to estimate of trajectory and terminal settling velocity of volcanic ash is presented.

The proposed approach aims to:

- realize a lab-scale system to investigate sedimentation processes of volcanic ash;
- perform a large set of experiments in order to evaluate the trajectory and terminal settling

velocity of particles falling in the tank by means of a vision system and a dedicated image post processing tool;

- calibrate the experimental set-up and accurately estimate the uncertainty on particle position and velocity;
- verify the accuracy of some models available in literature.

Section II describes the principle of similarity used to fix the experiment, Section III the experimental set-up and the developed methodology, the results of measurements of trajectory and terminal settling velocity are shown in Section IV, and finally the discussions of the results and conclusions in Section V and VI.

II. The principle of similarity

Bearing in mind the laboratory scale of the experiment under consideration, it has to be considered that an experiment will resemble the real scenario if both share geometric, kinematic and dynamic similarities. This means that, in order to match the real scenario, the analogue prototype must have the same scaled shape (geometric similarity), the fluid flow of both the model and real scenario must undergo similar time (cinematic similarity), and the ratios of all forces acting on corresponding fluid particles and boundary surfaces in the two systems must be constant (dynamic similarity) [11]. If these conditions are achieved then the lab-scale prototype could be considered a satisfactory reproduction of the real scenario. The laboratory system is usually scaled by dimensionless parameters in a way that geometric, cinematic, and dynamic similarities are satisfied. These parameters can be evaluated applying Buckingham's π theorem which asserts that for a system described by n physical variables function of k independent physical quantities, the system can be expressed by $p = n - k$ dimensional numbers constructed from the original variables. In our study (volcanic ash falling in atmosphere), the involved variables are the viscosity μ and the density ρ of the fluid, the size and speed V_T of the body and the drag force F_D which are all function of mass, length and time. From the Buckingham π theorem [12], it is possible to reduce the system from these five variables to two dimensionless parameters, the Reynolds number R_e and Drag coefficient C_D given by:

$$R_e = \frac{\rho V_T d}{\mu} \tag{6}$$

$$C_D = \frac{F_D}{\rho d^2 V_T^2}. \tag{7}$$

As C_D can be expressed as function of R_e, using the dimensional analysis we can transform a more complex system (five variables) into a system function of only one variable, the Reynolds number R_e. Terminal velocity of particles in the real scenario can be obtained by the terminal velocity of particles measured in the laboratory prototype under the following hypothesis:

$$R_e^{rs} = R_e^{lp} \tag{8}$$

where rs is for real scenario and lp is for laboratory prototype. Hence, using the same suffix for each physical quantity, we can write:

$$\frac{\rho^{rs}\ V_T^{rs}\ d^{rs}}{\mu^{rs}} = \frac{\rho^{lp}\ V_T^{lp}\ d^{lp}}{\mu^{lp}}. \tag{9}$$

Preliminary tests were carried out in order to identify the fluid suitable for the realization of the experimental set-up. Based on terminal settling velocity evaluation [10] and considering particles having a density of $1500\ \mathrm{kg/m^3}$ and a size detectable from the instrument, we identified glycerine as being the best fluid. Using (9), it is hence possible to evaluate the diameter of a spherical particle falling in the tank having the diameter of a spherical particle falling in the air, if the fluid properties (density and viscosity) are known. As the principle of similarity is valid also for non-spherical particles, (8) and (9) are always applicable. A scale factor of about 500 was calculated in this test, which means that a particle having a diameter of $1\ \mathrm{mm}$ size falling in the atmosphere behaves equivalently to a particle having a diameter of $500\ \mathrm{mm}$ in glycerin.

III. Experimental set-up and developed methodology

A. Experimental set-up

A dedicated experimental set-up has recently been developed at the sedimentology laboratory of the Istituto Nazionale di Geofisica e Vulcanologia, sezione di Catania (INGV-CT). The system consists of a glass tank filled with glycerine, a vision system and a dedicated software tool for image processing. The choice of the fluid was crucial and was linked to the law of similarity described in the previous section, and to some physical features of the fluid, e.g. handiness, clearness. The tank has the height of $90\ \mathrm{cm}$ and a base of $60\ \mathrm{cm} \times 60\ \mathrm{cm}$ and set on a hard wood base $(80\ \mathrm{cm} \times 80\ \mathrm{cm} \times 2.5\ \mathrm{cm})$ so measurements were not affected by the wall effect and particles reached terminal settling velocity. In fact, a particle having a diameter of $6\ \mathrm{cm}$ and density of $1750\ \mathrm{kg/m^3}$ will reach the terminal settling velocity in the tank of glycerine after covering about $40\ \mathrm{cm}$. Four web-cams were located orthogonally to the tank on a rigid support to measure the 3D trajectory and terminal velocity of falling particles (Figure 1). They were also located in apposite lines and they were free to move with respect to the tank. The four commercially available web-cams were connected to PC by USB. The cams had a CMOS sensor with a resolution of 320×240 pixel and frame rate $30\ \mathrm{fps}$. Obviously the web-cams do not have an external trigger for the acquisition so the pictures are acquired in an asynchronous way. It is unlikely that two web-cams generate two snapshots at the same time $\bar{t}$ but using the epipolar geometry constraint [13], it is possible to reconstruct the corresponding points in the image trajectory. Hence, even if for a specific time $\bar{t}$, the image position of the particle by one of the two web-cams is missed, the position of the particle at time $\bar{t}$ may be estimated. Following the acquisition will be considered synchronous. Backlighting and white sheets of paper were attached to the sides of the tank and used in order to improve the contrast between particle and background and the diffusion of the light.

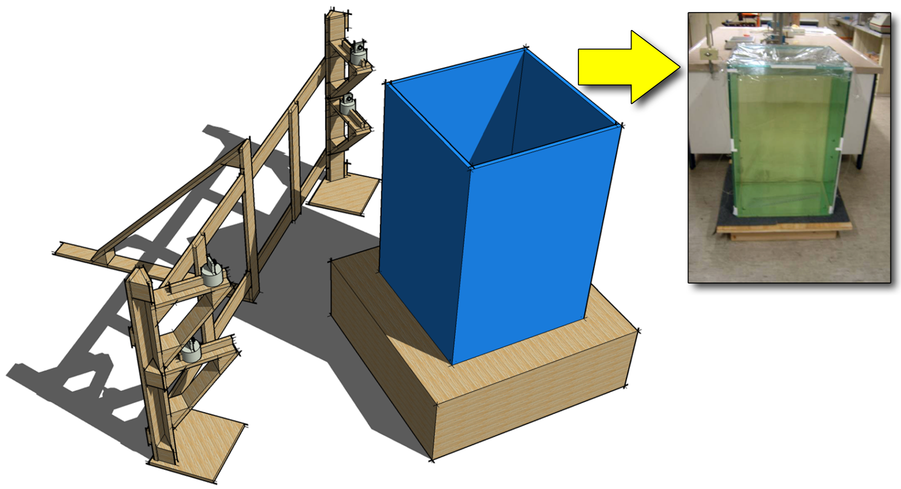

Fig. 1
LEFT: SCHEME OF THE EXPERIMENTAL SET-UP; RIGHT: TANK FILLED WITH THE GLYCERIN

B. The dedicated tool for image processing

A dedicated software tool was designed to acquire video sequences from each web-cam, save the sequence of frames, synchronize the frames, calibrate each web-cam and the experimental set-up, track and estimate the trajectory and velocity of the particles falling into the tank (Figure 2(a)). For each web-cam, the frame rate and the time were measured and visualized. The first section of the software allows to check all the web-cams and save the photograms in different folders, one for each web-cam, in which the time is written to distinguish among different experiments. A single video can be produced integrating the results of all web-cams. It is also possible to select a specific area (ROI, Region Of Interest) defined by the user. The acquired photograms are processed by a dedicated routine, in order to estimate the coordinates of the falling particle. The tool analyzed all the collected frames and reconstructed the trajectory and the velocity of the particles falling in the tank. Specific features of the IMAQ VISION toolbox of $LabVIEW^{TM}$ by National Instruments were exploited to this end. At the end of the elaboration the tool generated a basic report in which the area and the position of the rectangular region containing the particle for each frame were reported. The center of the particle was calculated by the intersection of the diagonals of the rectangular region the particle. A filter was also used to delete the noise due to shadow zones or faults during the acquisition. Figure 2(b) shows the front panel of the software developed in this work to acquire and elaborate experimental data.

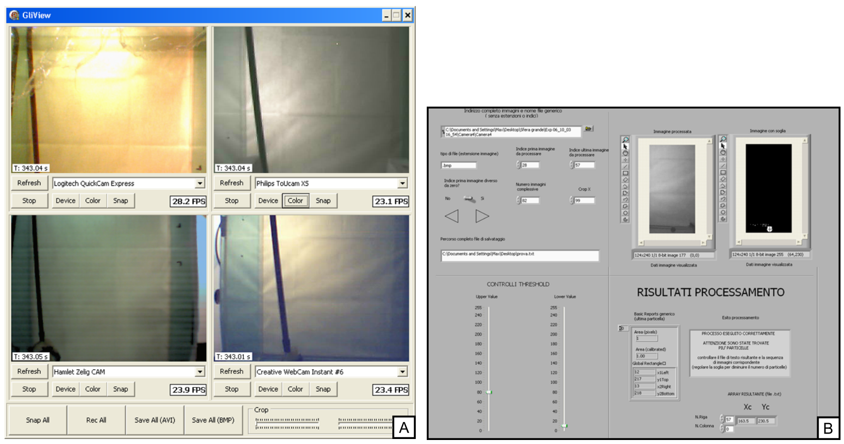

Fig. 2

SOFTWARE TOOLS FOR A) EXPERIMENT ACQUISITION AND B) ELABORATION

The calibration of the vision system was carried out in two steps. First, the calibration of each web-cam was based on the analysis of different frames of a dedicated pattern using the approach described in [14]. The second step was the calibration of the whole system to evaluate the position of each web cam with respect the other. In this case, the pattern was given simultaneously to all the four web-cams. The relative position and orientation of each camera was estimated with respect to the pattern by each camera model, and consequently with respect to the other web-cams. Thus the rototranslation matrix between each web-cam and the pattern is:

$$\mathbf{G}_i = \begin{bmatrix} \mathbf{R}_i & \mathbf{T}_i \\ 0 & 1 \end{bmatrix} \tag{10}$$

and between each web-cam and the other web-cams is:

$$\mathbf{M}_{ij} = \mathbf{G}_i \cdot \mathbf{G}_i^T \tag{11}$$

where $\mathbf{R}_i$ and $\mathbf{T}_i$ are respectively the attitude of the camera and the translation vector defining the position of the cameras with respect to the pattern (for details about the camera rototranslation matrix see [14]).

C. The estimation of the particle trajectory

The rototranslation matrices allow estimating the position of any object framed with respect to the web-cam or the pattern. To this end, it is necessary to evaluate the relation between the image planes and the spatial coordinates. For the detection of the 3D coordinates of a point $\mathbf{P}$ at the time $\bar{t}$, at least two web-cams must frame it at the time $\bar{t}$.

The relation between the image $\mathbf{i}_j$ of the point $\mathbf{P}$ in the j-th camera and spatial coordinates of $\mathbf{P}$ is function of the camera model matrix $\mathbf{K}_j$ and the rototranslation matrix $\mathbf{G}_j$:

$$\mathbf{i}_j = \mathbf{K}_j \cdot \begin{pmatrix} \mathbf{R}_j & \mathbf{T}_j \end{pmatrix} \cdot \begin{pmatrix} \mathbf{P} \\ 1 \end{pmatrix} = \mathbf{K}_j \cdot \mathbf{R}_j \cdot \mathbf{P} + \mathbf{K}_j \cdot \mathbf{T}_j. \tag{12}$$

In order to estimate the point $\mathbf{P}$ by the image point $\mathbf{i}_j$ equation (12) can be written:

$$\begin{aligned} &\mathbf{P}_j = \alpha_j \mathbf{R}_j^T \cdot \mathbf{K}_j^{-1} \cdot \hat{\mathbf{i}}_j - \mathbf{R}_j^T \cdot \mathbf{T}_j \\ &\mathbf{i}_j = \alpha_j \hat{\mathbf{i}}_j \\ &\hat{\mathbf{i}}_j = \begin{bmatrix} u_j & v_j & 1 \end{bmatrix}^T \end{aligned} \tag{13}$$

Equation (13) represents the parametric form (with parameter α_j) of a line passing through the center of the camera j-th and all points of this line generate the same image point $\mathbf{i}_j$. Using (13) and a multi view approach (see [14]) it is possible to estimate the position of the particle in the tank, and then the trajectory, and the relative uncertainty.

D. Uncertainty estimation

The uncertainty in the evaluation of the coordinates (x, y, z) of a particle is given by the intrinsic uncertainty of the measurement system, and the uncertainty introduced by the image processing. The intrinsic uncertainty of the measurement system was estimated in the following way: 50 frames having the pattern in different attitude were acquired for each couple of cameras and the 3D reconstruction of all points of the pattern was made in the reference system of the pattern. Since all the points of the pattern were known, it is possible to evaluate the uncertainty in the 3D reconstruction (Figure 3). It is notable that this kind of pattern allows a sub-pixel location of the chessboard corner points so the 3D reconstruction error was not affected by image processing error ([15] and [16]) .

	x	y	z
x	1.5995	−0.0149	0.9606
y	−0.0149	0.8166	−0.3612
z	0.9606	−0.3612	4.377

TABLE I
THE COVARIANCE MATRIX $\mathbf{\Omega}$ FOR TWO WEB-CAMS $[mm^2]$

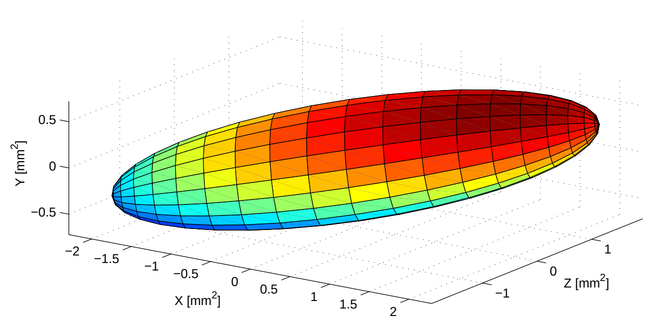

Fig. 3
UNCERTAINTY OF THE VISION SYSTEM IN THE RECONSTRUCTION OF THE REFERENCE PATTERN

In each experiment the 3D reconstruction was performed on 80 points and the experiment was repeated 50 times. The dataset allowed the estimation of the covariance matrix $\mathbf{\Omega}$ of the measurement system and confirmed that the uncertainty followed a Normal distribution. In the experiments, only the bottom web-cams, located in the region where particles reached their terminal velocity, were taken into account. Table I shows the covariance matrix $\mathbf{\Omega}$ for the two web-cams framing the lower part of the tank. It is notable that the uncertainty is smaller along the vertical dimension (axes y in the reference system of the camera).

Being $\mathbf{P}_j$ the estimations of a point $\mathbf{P}$ in the space obtained by WEB_j ($j = \{1, 2\}$), assuming that σ_i and σ_α are the uncertainties related to $\mathbf{i}_j$ and α_j respectively and using (13), the uncertainty estimation has been performed by applying general statistic approach for uncertainty propagation [17]:

$$\mathbf{\Lambda}_j = \mathbf{R}_j^T \mathbf{K}_j^{-1} \left(\sigma_\alpha^2 \mathbf{i}_j \mathbf{i}_j^T + \alpha_j^2 \sigma_i^2 \mathbf{I} \right) \mathbf{K}_j^{-T} \mathbf{R}_j \tag{14}$$

Combining the uncertainty of the two web-cams, the covariance matrix $\mathbf{\Lambda}$ in the estimation of $\mathbf{P}$ is given by:

$$\mathbf{\Lambda}^{-1} = \mathbf{\Lambda_0}^{-1} + \mathbf{\Lambda_1}^{-1} \tag{15}$$

Applying the inversion lemma

$$\begin{aligned} \mathbf{\Lambda} &= \left(\mathbf{\Lambda_0}^{-1} + \mathbf{\Lambda_1}^{-1} \right)^{-1} \\ &= \mathbf{\Lambda_0} - \mathbf{\Lambda_0} \cdot (\mathbf{\Lambda_0} + \mathbf{\Lambda_1})^{-1} \cdot \mathbf{\Lambda_0} \\ &= \mathbf{\Lambda_0} \cdot (\mathbf{\Lambda_0} + \mathbf{\Lambda_1})^{-1} \cdot (\mathbf{\Lambda_0} + \mathbf{\Lambda_1} - \mathbf{\Lambda_0}) \\ &= \mathbf{\Lambda_0} \cdot (\mathbf{\Lambda_0} + \mathbf{\Lambda_1})^{-1} \cdot \mathbf{\Lambda_1} \end{aligned} \tag{16}$$

The covariance matrix of the system is hence given by:

$$\mathbf{\Omega}_{sys} = \mathbf{\Omega} + \mathbf{\Lambda} \tag{17}$$

which represents the overall uncertainty on the estimation of $\mathbf{P}_j$.

Finally, considering the geometry of the tank and the quality of the tracking algorithm, the following standard deviations were obtained by performing experimental surveys on real targets:

$$\sigma_i = 2.6 \text{ pixel} \tag{18}$$

$$\sigma_\alpha = 200.0 \text{ mm} \tag{19}$$

By using the above described approach, after the system calibration it is possible to evaluate the uncertainty on the position of the particle, on the trajectory and finally on the terminal velocity. In particular the uncertainty on the particle settling velocity is:

$$\mathbf{\Omega}_{sv} = \frac{2}{\Delta t^2}\mathbf{\Omega}_{sys} \tag{20}$$

where Δt is the time observation interval and the uncertainty on his vertical component is:

$$\Omega_{vsv} = \mathbf{v}^T \cdot \mathbf{\Omega}_{sv} \cdot \mathbf{v} \tag{21}$$

where $\mathbf{v}$ is the vertical direction unit vector.

This approach has been applied to results presented in section IV obtaining the uncertainty given in table IV.

IV. RESULTS

Volcanic particles have an abundance of vesicles due to the exolution of magmatic gas [18] and could have a smaller density with respect to the glycerine. Hence, experiments were carried out with particles obtained using wax prints filled with a mixture of cement and laterite. Three synthetic particles (Figure 4) were realized and their density was measured using a Mohr-Westphal balance (Table II). These particles were dropped into the tank a few centimeters above the surface of the glycerin and the particle motion was registered by each web-cam with the dedicated software tool previously described.

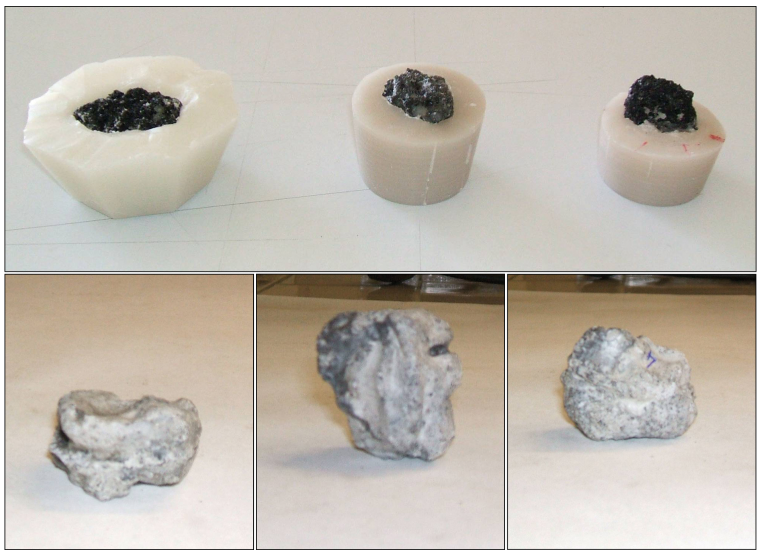

Fig. 4
PRINTS OF VOLCANIC PARTICLES

Particle	Density $(\mathrm{kg/m^3})$
Particle-1	1967.34
Particle-2	1700.57
Particle-3	2021.79

TABLE II
DENSITIES OF THE PRINTS

We also assessed the performance of the experimental set-up in predicting the actual behavior of particles by using spherical particles for which the settling law is given from the [10].

These particles were plastic spheres of different size, weight and density filled with sand (Table III). Their terminal settling velocity was calculated with the theoretical model of [10] and

	Diameter (m)	Weight (kg)	Density (kg/m^3)
Sphere-1	$4.98e{-2}$	0.110	1704.87
Sphere-2	$5.98e{-2}$	0.194	1733.85
Sphere-3	$6.98e{-2}$	0.313	1758.12

TABLE III

SIZE, WEIGHT AND DENSITY OF THREE SPHERICAL PARTICLES FILLED WITH SAND.

	VTE (mm/s)	VKL (mm/s)	$\Delta\%$
Sphere-1	220.68 ± 8.83	230.22	4.14
Sphere-2	309.82 ± 12.45	310.96	0.37
Sphere-3	390.21 ± 16.00	379.45	2.84

TABLE IV

TERMINAL SETTLING VELOCITY MEASURED BY THE EXPERIMENTAL SET-UP VTE COMPARED WITH THESE OBTAINED BY THEORETICAL MODEL FOR SPHERICAL PARTICLES VKL, AND DIFFERENCE IN PERCENTAGE $\Delta\%$ BETWEEN THESE TWO VALUES.

compared with values obtained from our experimental set-up (Table IV). The good agreement between the experimental and computed velocities is notable. Several tests were carried out using the three prints (Figure 4 and Table II). For each particle, about thirty drops were carried out and terminal settling velocities were evaluated together with their uncertainty.

Firstly, we analyzed the matching between the predictions obtained by the model of [10] assimilating particles 1, 2, 3 to spheres with diameter 0.0279 mm, 0.0351 mm and 0.0297 mm respectively (Table V). Note the high value of $\Delta\%$ which also reaches 22%. This means that experimental results do not fit the theoretical model well. The model presented in [5] gives the results presented in (Table VI). In this case, the comparison between the experimental data and results obtained by the model in [5] shows a better agreement (Table VII).

	VTE (mm/s)	VKL (mm/s)	$\Delta\%$
Particle-1	139.93 ± 5.00	170.64	21.94
Particle-2	143.94 ± 5.27	161.59	12.26
Particle-3	174.89 ± 6.48	198.66	13.59

TABLE V

TERMINAL SETTLING VELOCITY OF THE PARTICLES MADE WITH MELTED WAX AND FILLED WITH A MIXTURE OF CEMENT AND LATERITE VTE COMPARED WITH THOSE OBTAINED BY THEORETICAL MODEL OF [10] FOR SPHERICAL PARTICLES VKL HAVING THE SAME EQUIVALENT DIAMETER, AND DIFFERENCE IN PERCENTAGE $\Delta\%$ BETWEEN THESE TWO VALUES.

	a	b	c	F
Particle-1	0.0342	0.0260	0.0186	0.6513
Particle-2	0.0425	0.0373	0.0345	0.8447
Particle-3	0.0383	0.0300	0.0280	0.7572

TABLE VI

PRINCIPAL AXES AND FORM FACTOR F ([5]) OF THE PARTICLES MADE WITH MELTED WAX AND FILLED WITH A MIXTURE OF CEMENT AND LATERITE

V. DISCUSSIONS

In the recent years, experimental studies have been carried out in order to analyze several mechanisms of explosive activity such as interaction water-magma [19], pyroclastic flows (currents of hot gas and rock) [20] and dynamics of gas-particle mixtures [21], which are hard to study during an ongoing eruption. Similarly, terminal settling velocities of volcanic ash are very difficult to measure due to the very small size of particles (< 2 mm). The experiment described in this paper has, hence, allowed to reproduce the free-fall process of volcanic ash in laboratory using particles made ad hoc which are easily detected in laboratory. However, it should be pointed out that the proposed approach does not consider effects of wind and other disturbances to the trajectory of volcanic ash. As they could have an important role on particle deposition, future studies should address these phenomena (e.g. wind tunnel experiments).

	VTE (mm/s)	VWH (mm/s)	$\Delta\%$
Particle-1	139.93	134.69	3.74
Particle-2	143.94	157.24	9.23
Particle-3	174.89	175.65	0.43

TABLE VII
TERMINAL SETTLING VELOCITY OF THE PARTICLES MADE WITH MELTED WAX AND FILLED WITH A MIXTURE OF CEMENT AND LATERITE VTE COMPARED WITH THOSE OBTAINED BY THE THEORETICAL MODEL OF [5], AND DIFFERENCES IN PERCENTAGE $\Delta\%$ BETWEEN THESE TWO VALUES.

The proposed study is very important because it will allow improving our understanding on terminal settling velocity of volcanic ash. This factor influences several processes that take place in volcanic clouds and that are still unknown. Indeed, terminal settling velocity affects the efficiency of aggregation phenomena, typically for particles having diameters $< 100\mu\mathrm{m}$ [22]. Aggregation may cause the premature deposition of particles [23] and, consequently, a variation in the thickness of the associated deposit [24] or presence of double maximum [25]. It may also promote hydrometeor formation processes in volcanic clouds and thus modify volcanic plume microphysics [26].

Although similar experiments have already been carried out by [5] and [8] we note that in this work: i) measurements were obtained with high precision thanks to the use of sophisticated vision systems and advanced software; the uncertainty on terminal velocity estimation is also evaluated allowing the complete characterization of the experimental set-up and the opportunity to observe the limits of our measurements; ii) most of the particles which were analyzed in our experiment, have a lower than 20 Reynolds number, very near to the real fine ash, whereas particles used in the experiment of [8] have a higher than 10^2 Reynolds number.

Our results have shown that the terminal settling velocities measured experimentally differ up to 20% from those obtained by the theoretical model in which particles are assimilated to spheres. This is in agreement with values obtained by [6] and [9], highlighting again how the assumption of a spherical shape introduces systematic errors into models of tephra dispersal [9]. On the contrary, the comparison with the model of [5] showed a better agreement, with differences inferior to 10%. We also stress that our experimental results are comparable with results of Wilson and Huang's model because it is based on the simple particle shape descriptors (a, b and c being the axes of the particle in descending order) that are easy to measure by volcanologists.

In future, these experiments could improve the terminal velocity formulation through the use of the Best's number $Be = C_D Re^2$ [27], which allows evaluating the dependence of the drag coefficient in function of the Reynolds' number. This could be fundamental because terminal settling velocity plays an important rule on the results of tephra dispersal models such as HAZMAP [28], TEPHRA [29] and FALL3D [30]. Further, the uncertainty could be improved by fusing the measurements from multiple cameras with information fusion technology. In any case, it must be considered that even if the use of multiple cameras could improve the quantity of information, a more complicated image processing will be required which could also introduce other sources of uncertainty. Another possibility could be the use of high performance cameras. Certainly, a tradeoff between complexity and performance will also be taken into account.

VI. Conclusions

Several objectives were reached in this work: i) the realization of experiments that reproduce the real fallout scenario; ii) the development of software able to track the particle while it is falling in the tank and estimate the terminal settling velocity; iii) the reliable estimation of the uncertainty of terminal settling velocity; iv) the comparison between experimental terminal settling velocities and those calculated using two models available in literature. Our preliminary results encourage the implementation of further experiments using new prints of different shape. In future, new experiments will allow to find a parameterization of the terminal settling velocity formulation using simple shape descriptors. This will improve the results of volcanic ash dispersal models and hence contribute to reduce damages to aviation during explosive eruptions.

ACKNOWLEDGEMENTS

We thank Paola Del Carlo and Daniele Andronico who supported the realization of the experimental set-up in the laboratory of sedimentology at the Instituto Nazionale di Geofisica e Vulcanologia, sezione di Catania. We also thank three anonymous reviewers and the native English-speaker Stephen Conway. This research was supported by the FIRB Italian project ”Sviluppo Nuove Tecnologie per la Protezione e Difesa del Territorio dai Rischi Naturali” funded by Italian Ministry of Universities and Research for two authors (M. Prestifilippo and S. Scollo).

REFERENCES

[1] J. Fredsoe and R. Deigaard, *Mechanics of Coastal Sediment Transport (Advanced Series in Ocean Engineering)*, World Scientific Publishing Company, ISBN: 9810208413, 1992.

[2] R.P. Chhabra, L. Agarwal, and N.K. Sinha, “Drag on non-spherical particles in power law non-newtonian media,” *Powder Technology*, vol. 101, pp. 288 – 295, 1999.

[3] M. Bursik, *Tephra dispersal, In: Gilbert, J.S., Sparks, R.S.J. (Eds.), The Physics of Explosive Volcanic Eruptions*, vol. 145, pp. 115 – 144, Geological Society of London, 1998.

[4] G.P.L. Walker, “Grain-size characteristics of pyroclastic deposits,” *Journal of Geology*, vol. 79, pp. 696–714, 1971.

[5] L. Wilson and T.C. Huang, “The influence of shape on the atmospheric settling velocity of volcanic ash particles,” *Earth and Planetary Science Letters*, vol. 44, no. 2, pp. 311 – 324, 1979.

[6] C. M. Riley, W. I. Rose, and G. J. S. Bluth, “Quantitative shape measurements of distal volcanic ash,” *Journal of Geophysical Research*, vol. 108, no. B10, pp. ECV8.1 – ECV8.15, 2003.

[7] P.S. Roller, “Accurate air separator for fine powders,” *Industrial & Engineering Chemistry Analytical Edition*, vol. 3, no. 2, pp. 212 – 216, 1931.

[8] P. Dellino, D. Mele, R. Bonasia, G. Braia, L. La Volpe, and R. Sulpizio, “The analysis of the influence of pumice shape on its terminal velocity,” *Geophysical research letters*, vol. 32, no. 21, pp. L21306.1 – L21306.4, 2005.

[9] M. Coltelli, L. Miraglia, and S. Scollo, “Characterization of shape and terminal velocity of tephra particles erupted during the 2002 eruption of etna volcano, italy,” *Bulletin of Volcanology*, vol. 70, no. 10, pp. 1103–1112, 2008.

[10] D.K. Kunii and O. Levenspiel, *Fluidizzation Engineering*, John Wiley and Sons, New York, pp 97, 1969.

[11] S. Kline, *Similitude and Approximation Theory*, Springer-Verlag Berlin and Heidelberg GmbH & Co. K, ISBN: 0387165185, 1986.

[12] E. Buckingham, “The principle of similitude,” *Nature*, vol. 96, no. 2406, pp. 396 – 397, 1915.

[13] O. Faugeras, *Three-Dimensional Computer Vision*, MIT Press, ISBN: 9780262061582, 1993.

[14] R. I. Hartley and A. Zisserman, *Multiple View Geometry in Computer Vision*, Cambridge University Press, ISBN: 0521623049, 2000.

[15] V. Douskos, I. Kalisperakis, and G. Karras, “Automatic calibration of digital cameras using planar chess-board patterns,” in *Optical 3-D Measurement Techniques VIII (Wichman)*, 2007, vol. 1, pp. 132–140.

[16] J.-Y. JBouguet, “Camera calibration toolbox for matlab,” `http://www.vision.caltech.edu/bouguetj/calib_doc/`.

[17] JCGM 100:2008, “Evaluation of measurement data - guide to the expression of uncertainty in measurement,” `http://www.bipm.org/utils/common/documents/jcgm/JCGM_100_2008_E.pdf`.

[18] P. Dellino and L. La Volpe, “Image processing analysis in reconstructing fragmentation and

transportation mechanisms of pyroclatic deposits. the case of monte pilato-rocche rosse eruptions, lipari (aeolian islands, italy)," *Journal of Volcanology and Geothermal Research*, vol. 71, pp. 13–29, 1996.

[19] A. Austin-Erickson, R. Buettner, P. Dellino, M. Ort, and B. Zimanowski, "Phreatomagmatic explosions of rhyolitic magma: Experimental and field evidence," *Journal of Geophysical Research*, vol. 113, 2008.

[20] P. Dellino, B. Zimanowski, R. Buettner, L. La Volpe, and Sulpizio R. Mele, D., "Large-scale experiments on the mechanics of pyroclastic flows: Design, engineering, and first results," *Journal of Geophysical Research*, vol. 113, 2007.

[21] K. Chojnicki, A.B. Clarke, and J.C. Phillips, "A shock-tube investigation of the dynamics of gas-particle mixtures: Implications for explosive volcanic eruptions," *Geophysical Research Letters*, vol. 33, 2006.

[22] J.S Gilbert and S.J. Lane, "The origin of accretionary lapilli," *Bulletin of Volcanology*, vol. 56, no. 14, pp. 398–411, 1994.

[23] S.N. Carey and H. Sigurdsson, "Influence of particle aggregation on deposition of distal tephra from the may 18, 1980, eruption of mount st-helens volcano," *Journal of Geophysical Research*, vol. 87, no. 14, pp. 7061–7072, 1982.

[24] S.N. Bonadonna and J.C. Phillips, "Sedimentation from strong volcanic plumes," *Journal of Geophysical Research*, vol. 108, pp. 2340–2368, 2003.

[25] P. Armienti, G. Macedonio, and M.T Pareschi, "A numerical-model for simulation of tephra transport and deposition - applications to may 18, 1980, mount-st-helens eruption," *Journal of Geophysical Research*, vol. 93, pp. 6463–6476, 1988.

[26] A.J. Durant, W.I. Rose, A.M. Sarna-Wojcicki, S. Carey, and A.C.M. Volentik, "A numerical-model for simulation of tephra transport and deposition - applications to may 18, 1980,

mount-st-helens eruption," *Journal of Geophysical Research*, vol. 114, 2009.

[27] A.C. Best, "Empirical formulae for the terminal velocity of water drops falling through the atmosphere," *Quart. J. Roy. Meteor. Soc.*, vol. 76, pp. 302–311, 1950.

[28] G. Macedonio, A. Costa, and A. Longo, "A computer model for volcanic ash fallout and assessment of subsequent hazard," *Computers & Geosciences*, vol. 31, 2005.

[29] C. Bonadonna, C.B. Connor, and Connor L. Byrne M. Laing A. Hincks T.K. Houghton, B.F., "Probabilistic modeling of tephra dispersal: Hazard assessment of a multiphase rhyolitic eruption at tarawera, new zealand," *Journal of Geophysical Research*, vol. 110, 2005.

[30] A. Folch, C. Cavazzoni, and Macedonio G. Costa, A., "An automatic procedure to forecast tephra fallout," *Journal of Volcanology and Geothermal Research*, vol. 177, 2008.